46th AIAA Aerospace Sciences Meeting and Exhibit
7 - 10 January 2008, Reno, Nevada

AIAA 2008-744

Numerical Simulation of Planetary Reentry Aeroheating over Blunt Bodies with Non-equilibrium Reacting Flow

Akshay Prakash[1] and Xiaolin Zhong[2]

University of California, Los Angeles, California, 90095

Thermal protection layer has been commonly used to protect the reentry vehicles from the harsh conditions encountered at hypersonic velocities. Numerical simulations and experiments are used to predict the amount of this protective layer needed so that vehicles safely traverse the harsh zone. Prediction of ablation requires modeling of hypersonic flows coupled with reacting gas chemistry and the response of the solid protection layer to the extreme conditions. Codes doing chemistry with supersonic flow are coupled with codes predicting the response of the protection layer. However it would be more useful to integrated codes which solve both the hypersonic flow and the response of the surface to such flows. Therefore it is our aim to develop an integrated code which solves the material response along with the flow with non equilibrium chemistry, vibrational excitation, species dissociation and ionization. For the present paper we present our preliminary results from a high order Navier Stokes solver which includes non-equilibrium reaction flow with two temperature vibrational energy model.

I. Introduction

Prediction of the ablative thermal response of the ablative Thermal Protection Layer has been a subject of study since 1960s. Earliest efforts include the CMA [15] code (Charring Material Ablation) developed by Aerotherm Corporation in the late 1960s combined with the BLIMP (Boundary Layer Integral Matrix Procedure). This approach is characterized by solving the governing equations in solid (the TPS) using codes like 1-D CMA and in the fluid region (the gaseous environment, Integral Boundary Layer approach) separately using an independent code and the coupling the two solvers loosely through boundary conditions. Kuntz et. al. [10] along similar lines developed an iterative algorithm involving SACCARA and COYOTE which results in better convergence. SACCARA is a CFD code based on Steger Warming flux splitting and TVD flux function of Yee [25]. The solver is 2^{nd} order accurate in space discretization. It includes two-temperature model of Park [17 and 18] with vibration relaxation and chemical non equilibrium with 5 species model. COYOTE solves heat conduction and other diffusive problems. The solution procedure is based on Galerkin Finite Element Method. Finite Element Method makes the code suitable to model geometrically complex structures. COYOTE supports internal heat generation, convective and radiative boundary conditions and material properties as a function of temperature. The authors made various modifications to include support for abating surfaces and position dependent flux boundary condition. Murray and Russel [16] used MASCC (Maneuvering Aerotherm Shape Change Code) with CMA. MASCC is based on a boundary layer scheme MEIT (Momentum/Energy Integral Technique) and is a completely general three dimensional flow field solver which uses semi-empirical procedures to determine the flow field. Milos and Chen [3, 4, 5, 6, 13, and 14] have been developing surface chemistry models and computer codes for both 2-D and 3-D ablation and thermal response simulations. Recently they

[1] Student, Mechanical and Aerospace, akshay@seas.ucla.edu
[2] Professor, Mechanical and Aerospace, Associated Fellow, AIAA, xiaolin@seas.ucla.edu

developed a 3-D thermal response code 3dFIAT [6] for charring materials. Suzuki et. al. [24] have developed CFD methods for aero heating problems of ablating heat shields. The CFD code is coupled with the 1-D Aerotherm CMA code for material thermal responses.

Numerical prediction of ablation is challenging due to the complex multi-disciplinary physical and chemical processes that occur. In general, when subject to a large heat flux or elevated temperatures, thermal protection materials are affected by a combination of the following processes: pyrolysis, ablation of mechanical failure. Pyrolysis or thermal decomposition is the chemical decomposition in the interior of a material that releases gaseous by-products without consuming atmospheric species. Ablation is a combination of vaporization, sublimation, and reaction (such as oxidation and nitridation) which convert liquid of solid surface species into gaseous species. The liquid species would be a result of the material melting. Mechanical failure is the loss of surface material which does not produce gaseous species such as melt flow of a surface oxide, spallation of a solid and erosion caused by shear forces of impact of particles of droplets. For the current study we assume that 'ablation' only comprises of gaseous mass ejected from the surface without any surface recession. Surface recession would be added later. Such a case would be valid for TPS materials like carbon phenolic and Kevlar epoxy composites which release pyrolysis gases and form carbonaceous char layer.

These processes are a result of the hypersonic flow field which surrounds the vehicle. At such speeds the air is heated to temperatures high enough that real gas effects such as chemical decomposition and possibly ionization of the air becomes a significant factor in the analysis. So in the boundary layer adjacent to the surface of the vehicle the non-equilibrium chemical reactions between constituent elements of the air mixture need to be modeled. This requires that when numerically modeling the non-equilibrium chemically reacting boundary layer flow problem, multi-species kinetics and transfer properties be included, increasing the complexity of the analysis considerably. Now including ablation, the problem becomes coupled. Not only are the chemical reactions between the different species in the pyrolysis gas mixtures important but also their reactions with the various species in the boundary layer flow must be considered.

It is our aim to develop an intrinsically coupled CFD code for solving the flow field and the TPS thermal response. Such a code would be robust and highly accurate and would hence improve the efficiency of hypersonic flights. Considering the complexity of the problem we will develop the code in phases. In the first phase we aim to develop a high order non-equilibrium flow solver loosely coupled with an ablation thermal response code STAB II. In the next two phases we would develop an ablation thermal response code intrinsically coupled to the Navier Stokes solver. In this paper we present the results of the high order non-equilibrium flow solver with two temperature vibration relaxation.

II. Methodology

A. Governing Equations

The governing equations are essentially the Navier Stokes equations which assume a Newtonian gas flow model:

$$\frac{\partial \mathrm{U}}{\partial \mathrm{t}}+\frac{\partial \mathrm{F_j}}{\partial \mathrm{x_j}}+\frac{\partial \mathrm{F_{vj}}}{\partial \mathrm{x_j}}=\mathrm{w} \tag{1}$$

The flux is split into viscous and inviscid flux. The viscous flux consists of the diffusive flux whereas the inviscid flux is the convective flux. Where vector $U=[\rho_i, \rho u, \rho v, \rho w, Ev_i, E]$. First five rows in (1) represent the mass conservation equations, next three are momentum equations, and next three vibration energy conservation equations and last one is energy conservation equation. There is a source term due to thermo chemical non-equilibrium consisting of five species source terms and three vibration energy source terms. Viscous and inviscid flux and the source terms can be written as:

$$F_j=\begin{bmatrix}\rho_1 u_j\\ \rho_1 u_j\\ \rho_{NS} u_j\\ \rho u_1 u_j + p\delta_{1j}\\ \rho u_2 u_j + p\delta_{2j}\\ \rho u_3 u_j + p\delta_{3j}\\ E_{vM} u_j\\ (E+p)u_j\end{bmatrix};\quad F_{vj}=\begin{bmatrix}\rho_1 u_{1j}\\ \rho_1 v_{ij}\\ \rho_{NS} v_{NSj}\\ \tau_{j1}\\ \tau_{j2}\\ \tau_{j3}\\ k_{vM}\dfrac{\partial T_{vM}}{\partial x_j}+\rho e_{vM} D_M \dfrac{\partial c_M}{\partial x_j}\\ \tau_{ji}u_i + k\dfrac{\partial T}{\partial x_j}+\sum_M k_{vM}\dfrac{\partial T_{vM}}{\partial x_j}+\sum_s \rho_s h_s v_s\end{bmatrix};\quad w=\begin{bmatrix}w_1\\ w_i\\ w_{NS}\\ 0\\ 0\\ 0\\ Q_{T-v}+Q_{v-v}+w_M e_{vM}\\ 0\end{bmatrix} \tag{2}$$

$$\tau_{ij}=\mu\left(\frac{\partial u_i}{\partial x_j}+\frac{\partial u_j}{\partial x_i}\right)-\frac{2}{3}\mu\frac{\partial u_k}{\partial x_k}\delta_{ij} \tag{3}$$

The source term for vibration energy consists of translation to vibration exchange, vibration to vibration energy exchange and due to creation of diatomic species due to chemical reaction.

In (3) μ is the viscosity of the mixture determined from μ_s, the species viscosity through Wilke's [26] mixing rule. The species viscosity μ_s is determined by the Blottner's model [1]:

$$\mu_s = 0.1\exp\left[\left(A_s\ln(T)+B_s\right)\ln(T)+C_s\right]\quad (kg/ms) \tag{4}$$

Constants A, B and C are mentioned in Table 1 in appendix. Viscosity for mixture μ is calculated using Wilke's [26] mixing rule:

$$\mu=\sum_s\frac{X_s\mu_s}{\phi_s},\quad X_s=\frac{c_s M}{M_s},\quad M=\left(\sum_s\frac{c_s}{M_s}\right)^{-1} \tag{5}$$

$$\phi_s=\sum_r X_r\left[1+\sqrt{\frac{\mu_s}{\mu_r}}\left(\frac{M_r}{M_s}\right)^{1/4}\right]^2\left[\sqrt{8\left(1+\frac{M_s}{M_r}\right)}\right]^{-1} \tag{6}$$

The species u_{sj} velocity can be split into convective and diffusive velocities as [1]:

$$u_{sj}=v_{sj}+u_i \tag{7}$$

Note that j denotes the coordinate variable and s denotes the specie, v_{sj} is the diffusion velocity calculated using the Ficks law:

$$\rho_s v_{js}=\rho D_s\frac{\partial c_s}{\partial x_j};\quad c_s=\frac{\rho_s}{\rho};\qquad Le=\frac{D\rho c_p}{k} \tag{8}$$

Here D_s is the species diffusion coefficient calculated based on Lewis number Le which is assumed to be constant equal to 1 for all species for the present cases we have assumed that the diffusion coefficient is same for all the species.

B. Chemical Reaction Model

We have considered 5 species model of Park. Air predominantly consists of N_2 and O_2. For temperatures up to 9000 K air dissociates and forms N, O and NO. Composition of NO in the mixture peaks at about 3500 K. At 9000K we expect N and O in the mixture with traces of other species. Since for the present case we do not include ablation or surface chemistry, a five species model would be sufficient. Also note that the stagnation temperature is about 12000 K for the cases that we have considered. We consider the following reactions [1]:

$$\begin{aligned}
&1.\quad N_2 + M \Leftrightarrow 2N + M \\
&2.\quad O_2 + M \Leftrightarrow 2O + M \\
&3.\quad NO + M \Leftrightarrow N + O + M \\
&4.\quad N_2 + O \Leftrightarrow NO + N \\
&5.\quad NO + O \Leftrightarrow O_2 + N
\end{aligned} \tag{9}$$

The reaction rates can be written as:

$$\begin{aligned}
R_1 &= \sum_m \left[-k_{f_{1m}} \frac{\rho_{N_2}}{M_{N_2}} \frac{\rho_m}{M_m} + k_{b_{1m}} \frac{\rho_N}{M_N} \frac{\rho_N}{M_N} \frac{\rho_m}{M_m} \right] \\
R_2 &= \sum_m \left[-k_{f_{2m}} \frac{\rho_{O_2}}{M_{O_2}} \frac{\rho_m}{M_m} + k_{b_{2m}} \frac{\rho_O}{M_O} \frac{\rho_O}{M_O} \frac{\rho_m}{M_m} \right] \\
R_3 &= \sum_m \left[-k_{f_{3m}} \frac{\rho_{NO}}{M_{NO}} \frac{\rho_m}{M_m} + k_{b_{3m}} \frac{\rho_N}{M_N} \frac{\rho_O}{M_O} \frac{\rho_m}{M_m} \right] \\
R_4 &= -k_{f_{4m}} \frac{\rho_{N_2}}{M_{N_2}} \frac{\rho_O}{M_O} + k_{b_{4m}} \frac{\rho_{NO}}{M_{NO}} \frac{\rho_N}{M_N} \\
R_5 &= -k_{f_{5m}} \frac{\rho_{NO}}{M_{NO}} \frac{\rho_O}{M_O} + k_{b_{5m}} \frac{\rho_{O_2}}{M_{O_2}} \frac{\rho_N}{M_N}
\end{aligned} \tag{10}$$

And hence the species source terms are:

$$\begin{aligned}
w_{N_2} &= M_{N_2}(R_1 + R_4) \\
w_{O_2} &= M_{O_2}(R_2 - R_5) \\
w_{NO} &= M_{NO}(R_3 - R_4 + R_5) \\
w_N &= M_N(-2R_1 - R_3 - R_4 - R_5) \\
w_O &= M_O(-2R_2 - R_3 + R_4 + R_5)
\end{aligned} \tag{11}$$

The reaction rates were calculated using the following relations [19]:

$$\begin{aligned}
&k_{f_m}\left(\overline{T}\right) = C_{f_m} \overline{T}^{\eta m} \exp\left(-\theta_m / \overline{T}\right), \quad k_{b_m}\left(\overline{T}\right) = \frac{k_{f_m}}{k_{eq_m}} \\
&k_{eq_m} = \exp\left(A_{1m} + A_{2m} Z + A_{3m} Z^2 + A_{4m} Z^3 + A_{5m} Z^4\right), \quad Z = 10000/T \quad \text{T in K}
\end{aligned} \tag{12}$$

The values of reaction constants are given reference [19, 9] and in Table 3 and Table 4. The units for forward reaction rates are [cm^3/mole] and equilibrium reaction rates are in units consistent to these. Note that the forward reaction rates for reactions 1, 2 and 3 would be at a temperature that is the geometric mean of vibration and translational temperature. The reaction rates- backward and forward, for reactions 4 and 5 depend only on translation temperature. The backward reaction rates would depend on the translation temperature alone.

The source terms involving chemical reactions may become stiff, i.e. the rates for some reactions maybe orders of magnitude higher than the others. To overcome this we use implicit scheme for reacting source. For case of a well stirred reactor, the trapezoidal method of integration can be written as:

$$\left(I - \frac{\Delta t}{2}\left[\frac{\partial W}{\partial U} \right]^n \right)\left(U^{n+1} - U^n \right) = \Delta t \times W^n \tag{13}$$

Here $\frac{\partial W}{\partial U}$ is the Jacobean of the source term w.

C. Vibration Energy Model

The equation for vibration energy is solved in similar way to energy equation. The vibration energy is defined as [9, 22, 1]:

$$E_{vs} = \rho_s \frac{R}{M_s} \frac{\theta_{vs}}{e^{\theta_{vs}/T_v} - 1} \tag{14}$$

The values of θ_{vs} are listed in Table 2 in the appendix. There are three vibration energy terms each for the three diatomic species. Also note that unlike the energy term there is a source term which consists of vibration energy from translational energy and due to formation of diatomic species and from interaction between the diatomic species themselves. The vibration-vibration energy exchange is defined as [2]:

$$Q_{v-v\,s} = \sum_{r \neq s}^{s} \left[\hat{N} \sigma_{sr} \sqrt{\frac{8RT}{\pi \mu_{sr}}} \left(P_{sr} \frac{\rho_s}{M_s} E_{vr} - P_{rs} \frac{\rho_r}{M_r} E_{vs} \right) \right] \tag{15}$$

As we will see in the results, the vibration-vibration energy exchange is strongly coupled. Also note that the total energy term includes vibration energy and chemical energy terms. The total energy can be written as:

$$E = \sum_{s=1}^{NS} \rho_s c_{vs} T + \frac{1}{2} \sum_{s=1}^{NS} \rho_s u_i u_i + \sum_{s=1}^{m} E_{vs} + \sum_{s=1}^{NS} \rho_s h_s^0 \tag{16}$$

The exchange between vibration and translation energy can be calculated using [12, 20, 21, 22, and 23]:

$$Q_{T-v\,s_{L-T}} = \rho_s \frac{e_{vs}^*(T) - e_{vs}}{\left\langle \tau_{s_{L-T}} \right\rangle} \tag{17}$$

Where $\tau_{s\,LT}$ is the Landau Teller vibration relaxation given by [11, and 12]:

$$\left\langle \tau_{s_{L-T}} \right\rangle = \frac{\sum_r X_r}{\sum_r X_r / \tau_{sr_{L-T}}};$$

$$\tau_{sr_{L-T}} = \frac{1}{p} \exp\left[A_{sr} \left(T^{-1/3} - 0.015 \mu_{sr}^{1/4} \right) - 18.42 \right], \quad p \text{ in atm}; \tag{18}$$

$$A_{sr} = 1.16 \times 10^{-3} \mu_{sr}^{1/2} \theta_{vs}^{4/3}, \quad \mu_{sr} = M_s M_r / (M_s + M_r)$$

This however yields high values of the relaxation parameters and we use the modified formula by Park [22]:

$$Q_{T-v\,s_{L-T}} = \rho_s \frac{e_{vs}^*(T) - e_{vs}}{\tau_{vs}} \left| \frac{T_{shk} - T_{vs}}{T_{shk} - T_{vsshk}} \right|^{S_s - 1}$$
$$S_s = 3.5 e^{-\theta_s / T_{shk}} \tag{19}$$

And the relaxation parameter is given by Park [20]:

$$\tau_{vs} = \left\langle \tau_{s_{L-T}} \right\rangle + \tau_{cs} \tag{20}$$

Where,

$$\tau_{cs} = \frac{1}{c_s \sigma_v N_s};$$
$$c_s = \sqrt{8RT/\pi M_s}; \quad \sigma_v = 10^{-21} \left(50000/T\right)^2 [m^2] \tag{21}$$

D. Numerical Method

As mentioned in(1), flux is split into viscous and inviscid terms. Inviscid flux consists of convection terms while the viscous flux consists of the diffusive terms. These equations are transformed into body fitted curvilinear coordinates as in(22). Inviscid terms are flux split using Local Lax Friedrich's scheme and discretized using finite difference method. The source terms due to chemical reactions and vibration relaxation are put separately in 'w'.

$$\begin{cases} \xi = \xi(x,y,z) \\ \eta = \eta(x,y,z) \\ \varsigma = \varsigma(x,y,z) \\ \tau = t \end{cases} \Leftrightarrow \begin{cases} x = x(\xi,\eta,\varsigma,\tau) \\ y = y(\xi,\eta,\varsigma,\tau) \\ z = z(\xi,\eta,\varsigma,\tau) \\ t = \tau \end{cases} \tag{22}$$

Thus the governing equations become:

$$\frac{1}{J}\frac{\partial U}{\partial \tau} + \frac{\partial E'}{\partial \xi} + \frac{\partial F'}{\partial \eta} + \frac{\partial G'}{\partial \varsigma} + \frac{\partial E_v'}{\partial \xi} + \frac{\partial F_v'}{\partial \eta} + \frac{\partial G_v'}{\partial \varsigma} + U\frac{\partial\left(\frac{1}{J}\right)}{\partial \tau} = w \tag{23}$$

A fifth-order explicit finite difference scheme [27] is used for spatial discretization of the governing equations, the inviscid flux terms are discretized by the upwind scheme, and the viscous flux terms are discretized by 6th order central scheme. For the inviscid flux vectors, the flux Jacobeans contain both positive and negative eigenvalues, a simple local Lax-Friedrichs scheme is used to split vectors into negative and positive wave fields. For example, the flux term F′ can be split into two terms of pure positive and negative eigenvalues as follows:

$$F^{'} = F_{+}^{'} + F_{-}^{'}$$
$$F_{+}^{'} = \frac{1}{2}\left(F^{'} + \lambda U\right) \quad F_{-}^{'} = \frac{1}{2}\left(F^{'} - \lambda U\right) \tag{24}$$

Here λ is chosen to be larger than the local maximum of eigenvalues of $F^{'}$:

$$\lambda = \frac{|\nabla \eta|}{J}\left(\sqrt{\left(\varepsilon c\right)^2 + u^{'2}} + c\right) \tag{25}$$

Where $u^{'}$ is:

$$u' = \frac{\eta_x u + \eta_x v + \eta_x w}{|\nabla \eta|} \tag{26}$$

The parameter ε is a small positive constant added to adjust the smoothness of the splitting. The fluxes F'_+ and F'_- contain only positive and negative eigenvalues respectively. Therefore, in the spatial discretization of the differential equation, the derivative of the flux F' is split into two terms:

$$\frac{\partial F'}{\partial \eta} = \frac{\partial F_+'}{\partial \eta} + \frac{\partial F_-'}{\partial \eta} \tag{27}$$

The first term on the right hand side is discretized by the upwind scheme and the second term by the downwind scheme. The fifth-order explicit scheme utilizes a 7-point stencil and has an adjustable parameter α as follows [27]:

$$u_i' = \frac{1}{hb_i}\sum_{k=-3}^{3} a_{i+k}u_{i+k} - \frac{\alpha}{6!b_i}h^5\left(\frac{\partial u^6}{\partial^6 x}\right)_i + \ldots \tag{28}$$

$$\alpha_{i\pm3} = \pm 1 + \frac{1}{12}\alpha, \quad \alpha_{i\pm2} = \mp 9 - \frac{1}{2}\alpha, \quad \alpha_{i\pm1} = \pm 45 + \frac{5}{4}\alpha, \quad \alpha_i = 0 - \frac{5}{3}\alpha, \quad b_i = 60 \tag{29}$$

The scheme is upwind where $\alpha < 0$ and downwind when $\alpha > 0$. It becomes a six-order central scheme when $\alpha = 0$.

B. Shock Fitting

The solution procedure is base on shock fitting by Zhong [27]. The domain between the shock and blunt body is discretized and solved based on the Local Lax Friedrich flux splitting as discussed above. The conditions behind the shock are calculated using the Rankine Hugoniot relations:

$$\begin{aligned} &\left(\overrightarrow{F_s} - \overrightarrow{F_\infty}\right) \bullet \vec{l}_s + \left(U_s - U_\infty\right) l_t = 0 \\ &\vec{l}_s = \left(\frac{\eta_x}{J}\right)\vec{i} + \left(\frac{\eta_y}{J}\right)\vec{j} + \left(\frac{\eta_z}{J}\right)\vec{k} \\ &l_t = \left(\frac{\eta_t}{J}\right) \end{aligned} \tag{30}$$

The shock may be moving and its velocity (and hence the grid velocity) is calculated by differentiating the above expression in time and using the following compatibility relationships (31) and(32).

$$\begin{aligned} &\vec{l}_{N-1} \bullet \left[\frac{\partial(U/J)}{\partial \tau} + \frac{\partial F_1'}{\partial \xi} + \frac{\partial F_2'}{\partial \eta} + \frac{\partial F_3'}{\partial \zeta} - w\right] = 0 \\ &\vec{l}_{N-1} \bullet A_s' = \frac{|\nabla \eta|}{J}\left(u' + c\right)\vec{l}_{N-1} \end{aligned} \tag{31}$$

The shock is then advanced in time along with the flow governing equations.

E. Boundary Conditions

In shock fitting algorithm, the boundary at the shock is specified using Rankine Hugoniot relations with frozen gas assumption. Due to frozen gas assumption in the shock the composition of air behind the shock is identical to the free stream composition. The exit and the centerline have extrapolated values from the flow field. The boundary conditions on the solid surface depend on the nature of the problem. In the

intrinsically coupled solver that we plan to develop, the densities of various components would be dictated by the surface reactions; the temperature at the surface would be provided by the thermal response solver; pressure at the boundary would be such that gradients would be zero and velocity would be determined by the mass flow rate from the ablating surface. Currently we set the gradients of density and pressure to be zero corresponding to non catalytic wall. We can specify adiabatic or temperature specified conditions on the wall. Velocity is set to zero at the wall corresponding to the no slip condition.

$$\vec{l}_{N-1} = \begin{bmatrix} \frac{\gamma-1}{2}\left(\mathbf{u}.\mathbf{u} - h_1^0\right) - cu_n \\ \frac{\gamma-1}{2}\left(\mathbf{u}.\mathbf{u} - h_i^0\right) - cu_n \\ \frac{\gamma-1}{2}\left(\mathbf{u}.\mathbf{u} - h_{NS}^0\right) - cu_n \\ -\left(\frac{1}{2}cn_x - \frac{\gamma-1}{2}u\right) \\ -\left(\frac{1}{2}cn_y - \frac{\gamma-1}{2}v\right) \\ -\left(\frac{1}{2}cn_z - \frac{\gamma-1}{2}w\right) \\ \frac{\gamma-1}{2} \\ \frac{\gamma-1}{2} \end{bmatrix} \tag{32}$$

III. Results and Discussion

Current solvers loosely couple fluid flow solvers and thermal response code through boundary conditions. We present here the results of simulation of ideal gas flow over a spherical body and of non equilibrium flow over similar blunt body. The ideal gas flow simulation is over realistic sized geometry (~ 0.5 m). We also show the simulation of non equilibrium real gas flow. This includes the two temperature vibration energy model. This simulation was on a sphere of radius 3.81 x 10^{-3} m for an altitude of 50 km. The free stream conditions are taken from US STANDARD ATMOSPHERE. The ideal gas flow simulation was at Mach 10 and the non equilibrium was at Mach 15. For the present case we do not have surface chemistry hence a 5 specie model consisting of N_2, O_2, NO, N, O for reacting flow is sufficient. As a next step when we consider the surface chemistry or ablation, we would use 11 species model for reacting flow simulation consisting of $N_2, O_2, NO, N, O, C_3, C_2, CO, CN, C, C_2$. For the present case we can choose surface boundary conditions to be adiabatic or temperature specified with gradients of density and pressure set to zero. The ideal gas simulation was done for temperature specified boundary conditions while the reacting flow simulation was done for adiabatic wall conditions. In the non equilibrium flow the vibration temperature was set to the wall temperature with the assumption that the vibration temperature is in equilibrium with the surface temperature. Notice that in real gas simulation it is expected that vibration relaxation and chemical reaction would cause the temperature to decrease whereas in ideal gas flow the temperature along the stagnation line remain more or less constant.

A. Mach 10 Ideal Gas flow over a Blunt body

The flow over an axisymmetric spherical body (radius=0.5m) was simulated for free stream conditions of 46 km: $P_\infty = 1.313$ mili bars, $T_\infty = 266$ K , Mach 10 non reacting gas flow. The results are third order accurate in space and time. A low storage RK-3 method was used to advance in time.

Figure 1 shows the body fitted grid 200 x 160 on a spherical body. Figure 2 and Figure 3 show temperature and Mach contours. The boundary conditions at the wall is temperature specified ($T_{surface}$ = 1000K). Figure 2 shows temperature contours. We can see that the temperature is highest in the stagnation area and decreases as we move further from it. The highest temperature is about 5000 K. At 5000 K we expect all oxygen molecules to dissociate and air consists mainly of nitrogen and atomic oxygen with a little NO and N . Figure 3 shows Mach number contours. Figure 4 shows the temperature along the stagnation line. We see that the temperature is more or less constant except at the wall where we have temperature specified boundary condition $T = 1000K$. Note that $\eta = 0$ represents the surface and $\eta = 160$ represents the shock. Figure 5 shows velocity vectors and we can see that the vectors near the surface show a 'bump' before going to zero on the surface. It is expected the vectors would smoothly go to zero. This is because the boundary layer is not resolved at such a high Reynolds number. A finer grid is necessary near the boundary in spite of the large grid used.

B. Mach 15 Non-Equilibrium Flow Over Spherical Blunt Body

Simulation was done with the 5 species (N_2, O_2, NO, N, O) reaction model for the flow over a spherical blunt body using 80x60 grid. Free stream conditions are for 50 km altitude (from US STANDARD ATMOSPHERE): P_∞=79.77 Nt m^{-2}, ρ_∞ = 1.0275x 10^{-3} kg m^{-3}, $M_\infty = 15$. The initial composition and free stream composition of air was N2: 0.8; O2:0.17; NO: 0.01; O: 0.01; N: 0.01 (mass fractions). The results are third order accurate in time and space. For time advancement a low storage RK-3 scheme was used.

Figure 6 shows the mesh used for this simulation. The top half grid is 80X60. The grids are clustered near the surface and near the centerline in eta and zeta directions. Figure 7 shows the variation of temperatures along the centerline. The transitional temperature varies from about 12000 K immediately behind the shock to about 9000 K at the surface. The vibration temperatures vary from the free stream temperature of 270.7 K at shock to 9000 K at the surface. Vibration temperature at the wall was set to transitional-rotation temperature. Also note that the three vibration temperatures are very similar and a one vibration temperature model would be sufficient. Figure 8 shows the variation of temperatures at $\xi = 40$ and the three temperatures are very similar. Strong Vibration-Vibration coupling forces the vibration temperatures to be in equilibrium. For this simulation we used adiabatic boundary conditions and we can see that the surface temperature is indeed very high. At 9000 K the composition of air would be N and O with all the nitrogen, oxygen and NO dissociated. Figure 9 shows the composition of flow field along the centerline. Note that N_2 is a major component even at 9000 K though NO and O2 have completely dissociated. Also note that NO is in significant amounts some distance away from the surface. Figure 10 shows the temperature contours. The top half represents ideal gas flow and the bottom half non equilibrium flow. For the bottom half we can see that immediately behind the shock the temperature is the highest and then gradually decreases to the wall temperature while in the top half the temperature is uniform throughout the stagnation region. This is because chemical reactions and vibration relaxation reduce the temperature of the flow field. Figure 11 shows pressure contours, the top half for ideal gas flow and the bottom half for non equilibrium flow. The pressure is highest at the stagnation region and gradually decreases as we approach the exit. Note however that the pressure in lower half is less as compared to the top half though the contours are similar. Figure 12 represents Mach number contours. There is no difference in the Mach number contours in ideal and non equilibrium flow simulation. Figure 13 shows the prediction of shock standoff distance. The top half, ideal gas flow simulation predicts a larger value of shock distance than the lower half which is non equilibrium simulation. This is due to lower temperature in the flow field due to chemical reactions and vibration non equilibrium.

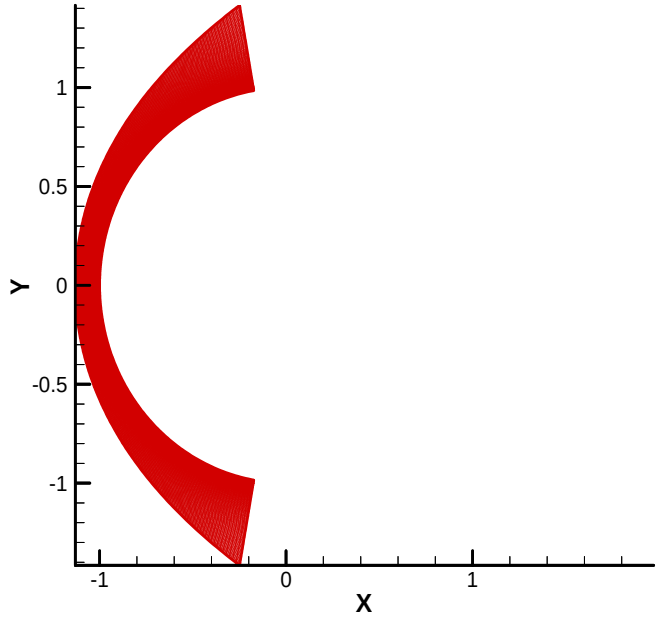

Figure 1: The mesh used for simulations: 200x160 grids for the top half. The relative scale of 0-1.0 measures for 0.5 m (actual geometry).

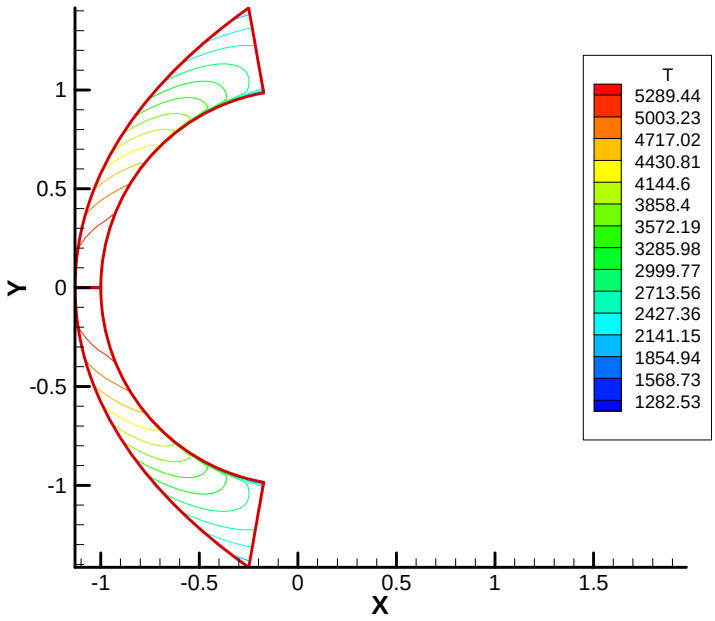

Figure 2: Temperature contours.

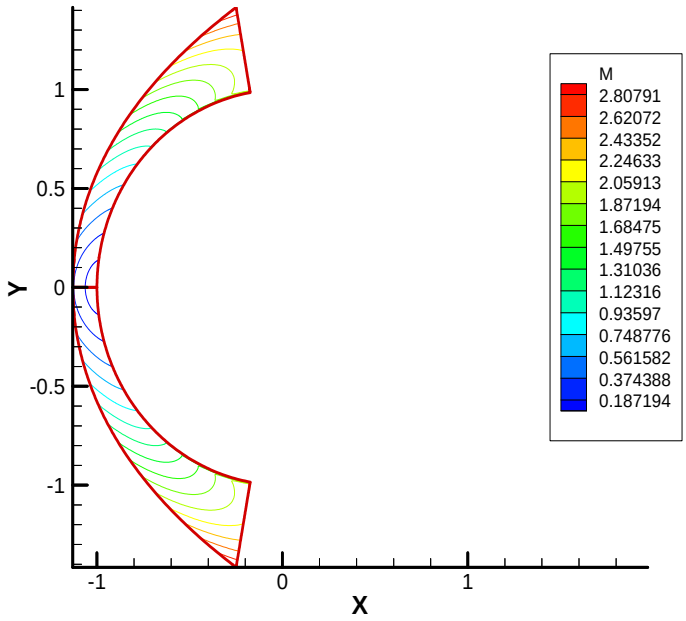

Figure 3: Mach number contours.

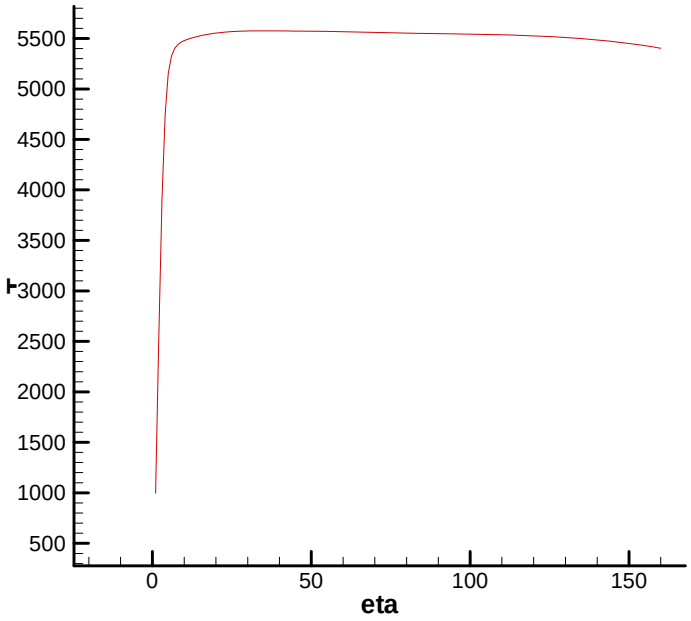

Figure 4: Temperature vs. η for ξ=1 (stagnation line)

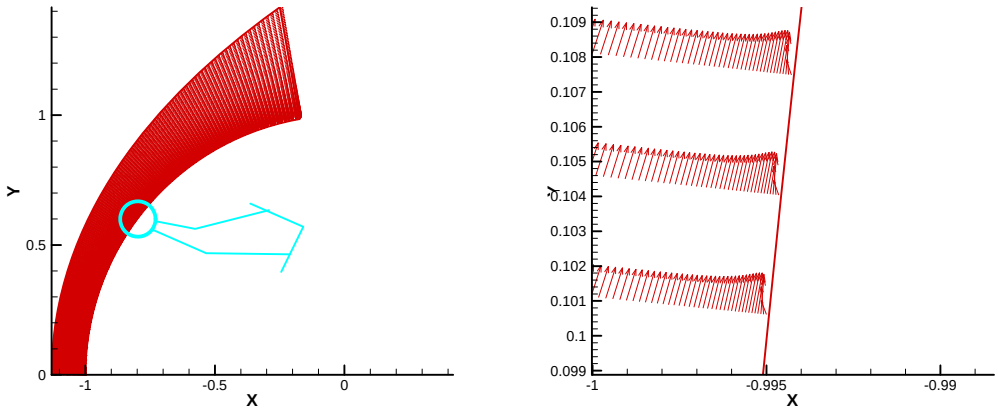

Figure 5: Velocity Vectors

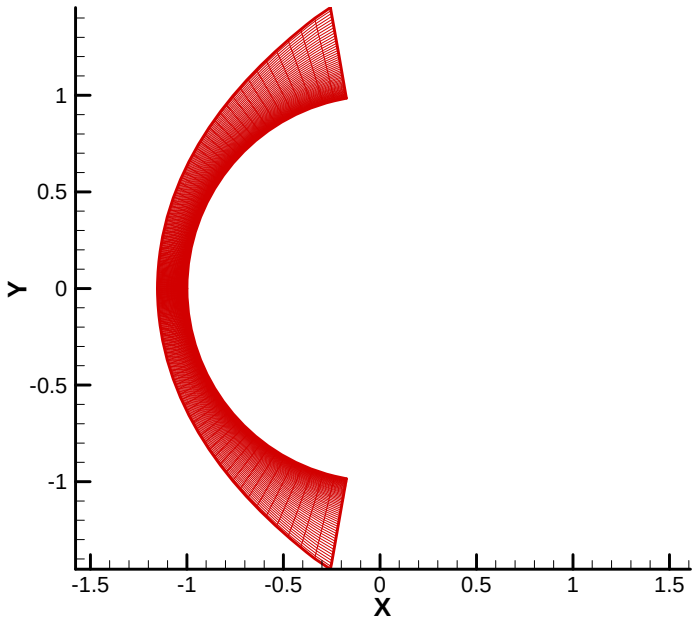

Figure 6: The mesh used for simulations: 80x60 grids for the top half. The relative scale of 0-1.0 measures for 3.81 x 10^{-3} ms

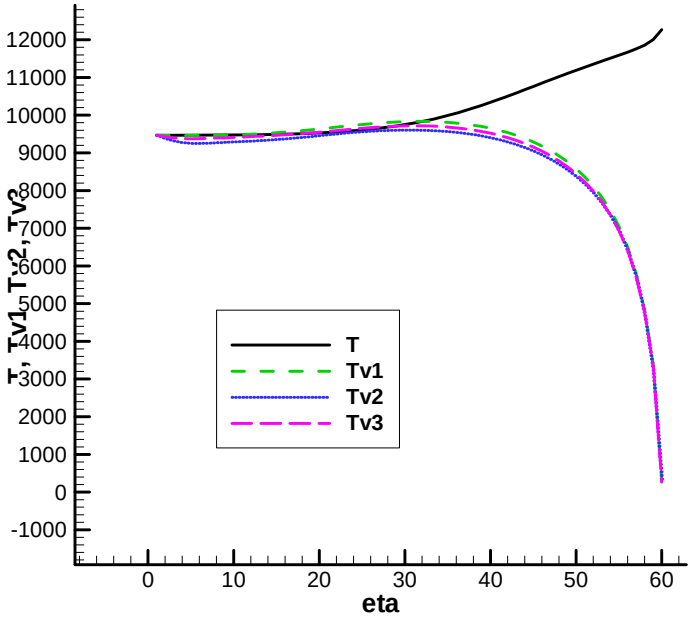

Figure 7: Distribution of vibration temperature along the centre line. Tv1 represents vibration temperature for N_2, Tv2 for O_2, and Tv3 for NO.

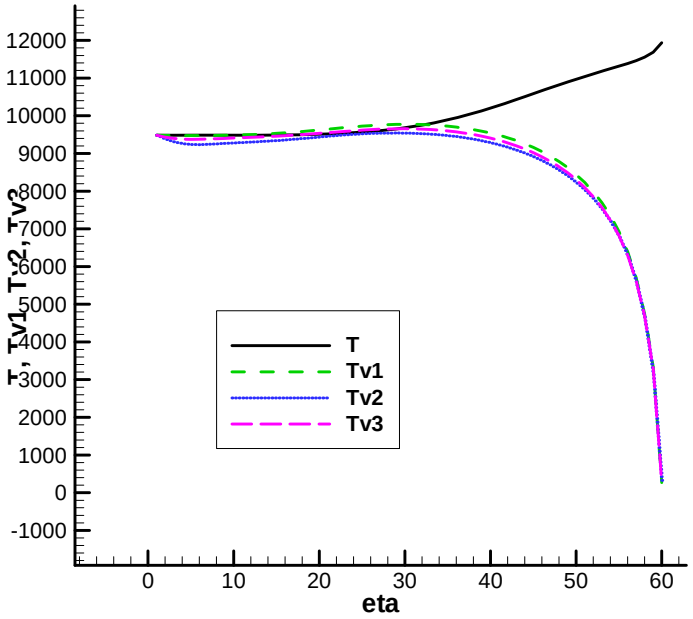

Figure 8: Distribution of vibration temperatures at zeta 40 (zeta varies from 1 to 60)

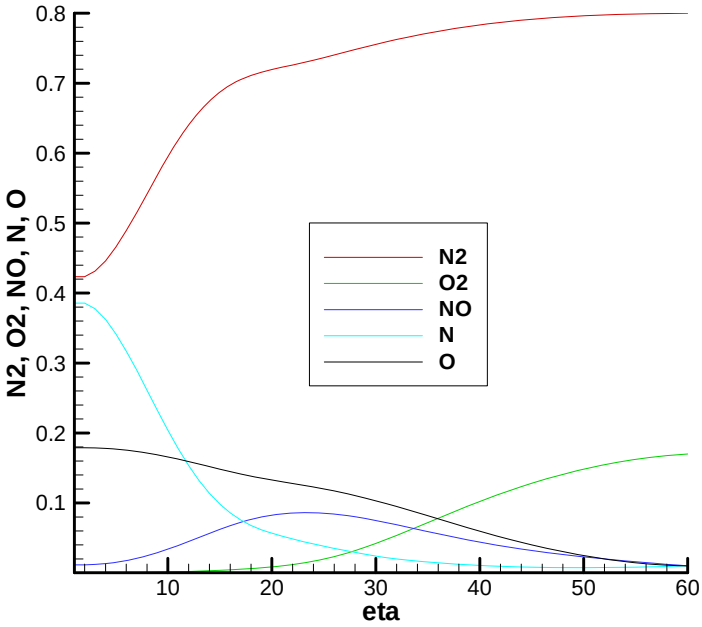

Figure 9: Mass fractions along the center line

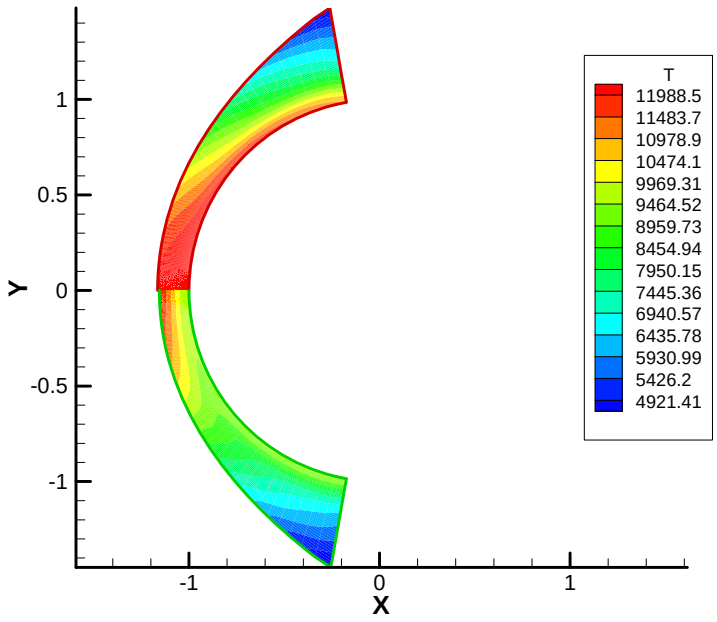

Figure 10: Temperature contours. Top half represents ideal gas flow and bottom half non equilibrium flow.

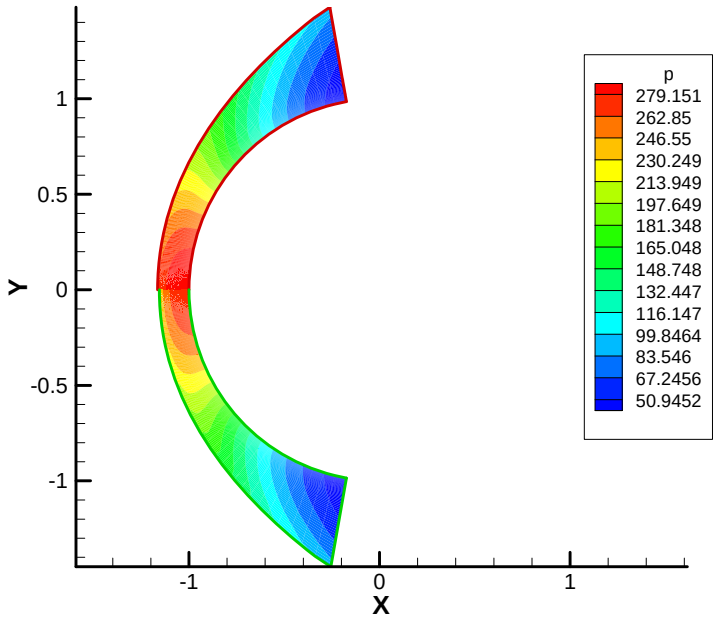

Figure 11: Pressure contours. Top half represents ideal gas flow and bottom half non equilibrium flow.

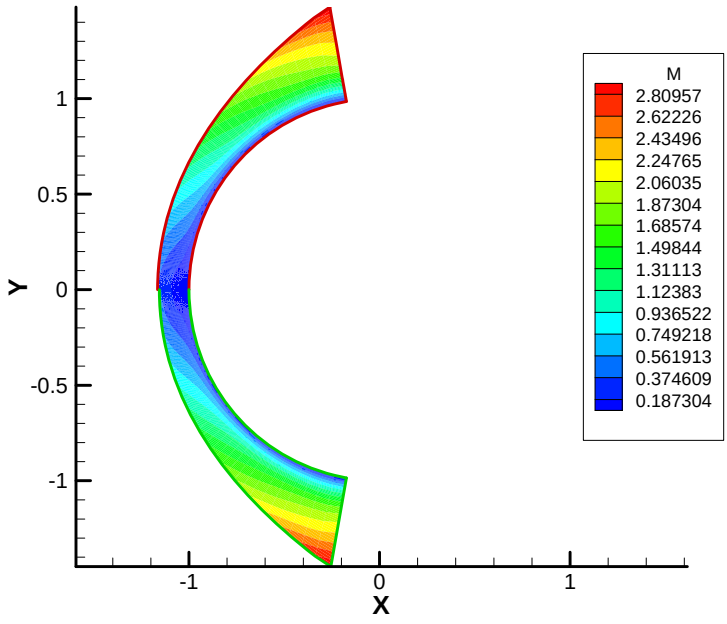

Figure 12: Mach number contours. Top half represents ideal gas flow and bottom half non equilibrium flow.

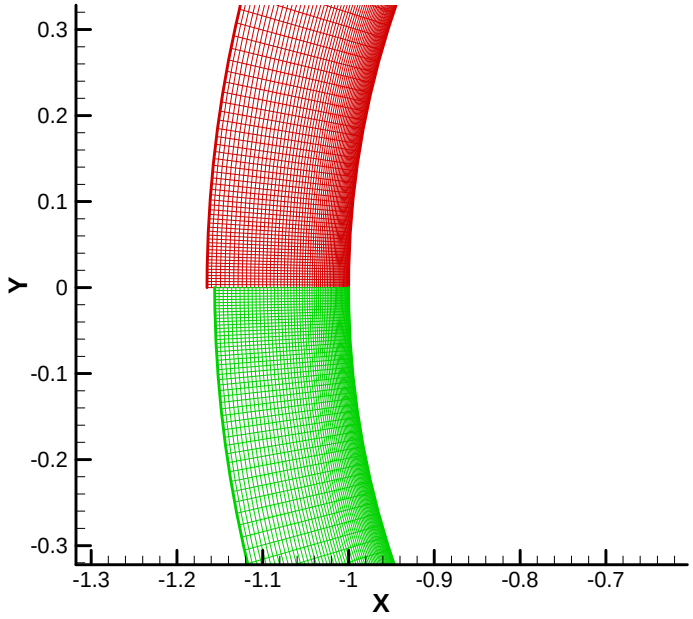

Figure 13: Shock standoff distance. Top half is ideal gas flow and bottom half is non equilibrium flow.

IV. Conclusion

The high order code based on shock fitting [27] was tested for high Mach number for ideal gas flow and flow with chemical and vibration non equilibrium and non catalytic surface. Vibration relaxation and chemical reactions are important phenomena that affect the flow at such high temperatures. These simulations are just the preliminary results for the Navier Stokes solver that would be used along with an ablation thermal response code. However to include ablation or even surface chemistry we need to include more species and currently we are developing 11 species version of the code consisting of $N_2, O_2, NO, N, O, C_3, C_2, CO, CN, C, C_2$, which has surface chemistry. Carbon is released into the flow field from the phenolic ablative material on the reentry vehicles. We are also working on coupling the code to STAB II, a one dimensional material thermal response code. We aim to develop an intrinsically coupled in-depth thermal response code and high order Navier Stokes solver based on Shock fitting method for hypersonic flow with surface ablation.

Any simulation for actual size vehicle would require the code to run on multiple processors. We plan to develop a parallel version of the code for faster simulations

Acknowledgements: The project was funded by NASA Dryden Research Center and is being monitored by Dr. William L. Ko, Leslie Gong and Bob Quinn of the NASA Dryden Research Center.

VI. References

1. Blottner, F.G., Johnson, M., and Ellis, M., Chemically Reacting Viscous Flow Program for Multi-Component Gas Mixtures. Report No. SC-RR-70-754, Sandia Laboratories, Albuquerque, New Mezico.
2. Candler, G.V., "The Computation of weakly ionized hypersonic flows in thermo chemical nonequilibrium", PhD thesis, June, 1988.
3. Chen, Y.K., Henline, W.D., Chemical nonequilibrium Navier-Stokes solutions for hypersonic flow over an ablating graphite nosetip. AIAA paper 93-2836, 1993.
4. Chen, Y.K., Henline, W.D., Hypersonic nonequilibrium Navier-Stokes solutions over an ablating graphite nosetip. Journal of Spacecraft and Rockets. 1994. 31(5): p. 728-734.
5. Chen, Y.K., Milos, F.S., Navier-Stokes Solutions with Finite Rate Ablation for Planetary Mission Earth Reentries Journal of Spacecraft and Rockets 2005. 42(6):p. 961-970.
6. Chen, Y.K., Milos, F.S., Three-Dimensional Ablation and Thermal Response Simulation Sys. AIAA paper 2005-5064 2005.
7. Conti, R.J., MacCormak, R.W., Groener, L.S., Fryer, J.M., Practical Navier Stokes computation of axis-symmetric reentry flow fields with coupled ablation and shape change AIAA paper 1992-752, 1992:p. 1-9.
8. Curry, D.M., An Analysis of a Charring Ablation Thermal Protection System. NASA TN D-3150, 1965.
9. Kruger, C. H., Vincenti, W. G., "Introduction to Physical Gas Dynamics", John Wiley and Sons, 1965.
10. Kuntz, D.W., Hassan, B., Potter, D.L., Predictions of Ablation Hypersonic Vehicles Using an Iterative Coupled Fluid/Thermal Approach. Journal of Thermophysics and Heat Transfer 2001. 15(2):p.129-139.
11. Lee, J.H., Basic Governing Equations for the Flight Regimes of Aeroassisted Orbital Transfer Vehicles. Thermal Design of Aeroassisted Orbital Transfer Vehicles, ed. H.F. Nelson, Progress in Aeronautics and Astronautics, 96, pp. 3-53, 1985.
12. Millikan, R.C., and White, D.R., Systematic of Vibrational Relaxation. J. of Chem. Phys. 39, pp. 3209-3213, 1963.
13. Milos, F.S., Rasky, D.J., Review of numerical procedures for computational surface thermo-chemistry. Journal of Thermophysics and Heat Transfer 1994. 8(1):p. 24-34.
14. Milos, F.S., Chen, Y.K., Comprehensive model for multi-component ablation thermo-chemistry. AIAA paper 1997-141, 1997.
15. Moyer, C. B. R., R. A., An Analysis of The Coupled Chemically Reacting Boundary Layer and Charring Ablator Part II Finite Difference Solution for the In-Depth Response of Charring Materials Considering Surface Chemical and Energy Balances. NASA CR-1061, 1966.
16. Murray, A.L., Russell, G.W., Coupled Aeroheating/Ablation Analysis for Missile Configurations. AIAA paper 2000-2587, 2000.
17. Park, C., Review of Chemical-Kinetic Problems of Future NASA Missions, I: Earth Entries, Journal of Thermophysics and Heat Transfer, Vol. 7, No. 3, 1993, pp. 384-398.
18. Park, C., Howe, J.T., Jaffe, R.L., and Candler, G.V., Review of Chemical-Kinetic Problems of Future NASA Missions II: Mars Entries, Journal of Thermodynamics and Heat Transfer, Vol. 8, No. 1, 1994, pp. 9-23.
19. Park, C., On Convergence of Computation of Chemically Reacting Flows. AIAA Paper no. 85-0247, 1985.
20. Park, C., Calculation of Nonequilibrium Radiation in the Flight Regimes of Aeroassisted Orbital Transfer Vehicles, ed. H.F. Nelson, Progress in Aeronautics and Aeronautics, 96, pp. 395-418, 1985.
21. Park, C., Assessment of Two-Temperature Kinetic Model for Dissociating and Weakly ionized Nitrogen. AIAA Paper No. 86-1347, 1986.
22. Park, C., Assessment of Two-Temperature Kinetic Model for Dissociating and Weakly ionizing Air. AIAA Paper No. 87-1574, 1987.

23. Parker, J.G., Rotational and Vibrational Relaxation in Diatomic Gasses. Physics of Fluids, 2, pp. 449-462, 1959.
24. Suzuki, T.S., Furudate, M., Sawada, K., Unified Calculation of Hypersonic Flow-field for a Reentry Vehicle. Journal of Thermophysics and Heat Transfer. 2002. 16(1): P. 94-100.
25. Yee, H.C., Implicit and Symmetric Shock Capturing Schemes, NASA TM-89464, May 1987.
26. Wilke, C.R., A Viscosity Equation for Gas Mixtures. Journal of Chem. Phys., 18, pp517-519 (1950)
27. Zhong, X., High-Order Finite-Difference Schemes for Numerical Simulation of Hypersonic Boundary-Layer Transition. Journal of Computational Physics, 144, 662-709 (1998).
28. Zhong, X. 1997a Direct numerical simulation of hypersonic boundary-layer transition over blunt leading edges. Part II: Receptivity to sound. AIAA Paper 97-0756.
29. Zhong, X. 1997b Direct numerical simulation of hypersonic boundary-layer transition over blunt leading edges, Part I: New numerical methods and validation. 35th AIAA - Aerospace Sciences Meeting and Exhibit, January 6–9, Reno, Nevada. AIAA Paper 97-0755.

Appendix

Table 1: Constants for calculating viscosity

	A_s	B_s	C_s
N_2	0.0268142	0.3177838	-11.3155513
O_2	0.0449290	-0.0826158	-9.2019475
NO	0.0436378	-0.0335511	-9.5767430
N	0.0115572	0.6031679	-12.4327495
O	0.0203144	0.4294404	-11.6031403

Table 2: Characteristic temperature for vibration model

Species	Θ_{vs}
N_2	3395
O_2	2239
NO	2817

Table 3: Coefficients in Eq. (12) for Equilibrium constant (k_{eq} units consistent with k_f)

Reaction No.	A1	A2	A3	A4	A5
1	3.898	-12.611	0.683	-0.118	0.006
2	1.335	-4.127	-0.616	0.093	-0.005
3	1.549	-7.784	0.228	-0.043	0.002
4	2.349	-4.828	0.455	-0.075	0.004
5	0.215	-3.657	0.843	-0.136	0.007

Table 4: Coefficients for Forward Rate Constants in Eq. (12) (k_f in cm^3/mole)

Reaction No.	Colliding partner	C_{fm}	η_m	Θ_m
1	N_2	$3.7x10^{21}$	-1.6	113200
	O_2	$3.7x10^{21}$	-1.6	113200
	NO	$3.7x10^{21}$	-1.6	113200
	N	$1.11x10^{22}$	-1.6	113200
	O	$1.11x10^{22}$	-1.6	113200
2	N_2	$2.7x10^{19}$	-1.0	59500
	O_2	$2.7x10^{19}$	-1.0	59500
	NO	$2.7x10^{19}$	-1.0	59500
	N	$8.2x10^{19}$	-1.0	59500
	O	$8.2x10^{19}$	-1.0	59500
3	N_2	$2.3x10^{17}$	-0.5	75000
	O_2	$2.3x10^{17}$	-0.5	75000
	NO	$2.3x10^{17}$	-0.5	75000
	N	$4.6x10^{17}$	-0.5	75000
	O	$4.6x10^{17}$	-0.5	75000
4		$3.18x10^{13}$	0.1	37700
5		$2.16x10^{8}$	1.29	19220